Physics of Plasmas

Probing ion species separation and ion thermal decoupling in shock-driven implosions using multiple nuclear reaction histories

Cite as: Phys. Plasmas **26**, 072703 (2019); https://doi.org/10.1063/1.5097605
Submitted: 26 March 2019 . Accepted: 12 June 2019 . Published Online: 29 July 2019

H. Sio, O. Larroche, S. Atzeni, N. V. Kabadi, J. A. Frenje, M. Gatu Johnson, C. Stoeckl, C. K. Li, C. J. Forrest, V. Glebov, P. J. Adrian, A. Bose, A. Birkel, S. P. Regan, F. H. Seguin, and R. D. Petrasso

Physics of Plasmas ARTICLE scitation.org/journal/php

Probing ion species separation and ion thermal decoupling in shock-driven implosions using multiple nuclear reaction histories

Cite as: Phys. Plasmas **26**, 072703 (2019); doi: 10.1063/1.5097605
Submitted: 26 March 2019 · Accepted: 12 June 2019 ·
Published Online: 29 July 2019

View Online Export Citation CrossMark

H. Sio,[1,a)] O. Larroche,[2] S. Atzeni,[3] N. V. Kabadi,[1] J. A. Frenje,[1] M. Gatu Johnson,[1] C. Stoeckl,[4] C. K. Li,[1] C. J. Forrest,[4] V. Glebov,[4] P. J. Adrian,[1] A. Bose,[1] A. Birkel,[1] S. P. Regan,[4] F. H. Seguin,[1] and R. D. Petrasso[1]

AFFILIATIONS

[1]Plasma Science and Fusion Center, Massachusetts Institute of Technology, Cambridge, Massachusetts 02139, USA
[2]CEA DAM DIF, 91297 Arpajon Cedex, France
[3]Dipartimento SBAI, Università degli Studi di Roma "La Sapienza," Via Antonio Scarpa 14, 00161 Roma, Italy
[4]Laboratory for Laser Energetics, Rochester, New York 14623, USA

[a)]hsio@mit.edu

ABSTRACT

Simultaneously measured DD, DT, and D^3He reaction histories are used to probe the impacts of multi-ion physics during the shock phase of inertial confinement fusion implosions. In these relatively hydrodynamiclike (burn-averaged Knudsen number $\langle N_K \rangle \sim 0.3$) shock-driven implosions, average-ion hydrodynamic DUED simulations are able to reasonably match burnwidths, nuclear yields, and ion temperatures. However, kinetic-ion FPION simulations are able to better simulate the timing differences and time-resolved reaction rate ratios between DD, DT, and D^3He reactions. FPION simulations suggest that the D^3He/DT reaction rate ratio is most directly impacted by ion species separation between the ^3He and T ions, whereas the D^3He/DD reaction rate ratio is affected by both ion species separation and ion temperature decoupling effects.

I. INTRODUCTION

Strong shock propagation plays an important role in energy transport in many astrophysical phenomena[1] and during the shock phase of inertial confinement fusion (ICF) implosions.[2] Average-ion, radiation-hydrodynamic codes[3,4] are typically used to model ICF implosions, but they only model an averaged ion species and assume a collisional plasma. The interactions between different ion species and deviations from hydrodynamic evolution are more pronounced during the shock phase of an ICF implosion, when ion-ion mean paths in the fuel are comparable to the fuel radius. Multi-ion and kinetic physics can lead to measurable changes in implosion performance such as yield degradation,[5] anomalous yield scaling,[6,7] ion thermal decoupling,[8] and ion species separation.[9,10] These multi-ion/kinetic effects related to the ion mean free path,[11] ion mass,[12] and ion charge[13] have been modeled using reduced ion-kinetic models,[14] particle-in-cell (PIC) simulations,[15–17] and kinetic-ion simulations.[18–22]

This work follows the experiments described by Sio *et al.*,[10] and greatly expands on this previous work through the inclusion of (1) two new experiments on DD and D^3He reaction histories, (2) one new experiment on DD, DT, and D^3He reaction histories, and (3) kinetic-ion FPION simulations in the interpretation of the data. There are significant experimental challenges in diagnosing the density and temperature differences between different ion species (ion species separation and ion thermal decoupling, respectively). With few exceptions,[10,23] the majority of existing experimental work investigating the role of kinetic and multi-ion physics in ICF implosions made use of time-integrated nuclear observables (reaction yields and ion temperatures). The experimental interaction signatures between the D, T, and ^3He ions are the DD, DT, and D^3He reactions and measurements of the DD, DT, and D^3He reaction histories using the Particle X-ray Temporal Diagnostic (PXTD)[24] enable time-resolved studies of these multi-ion effects. In this work, time-resolved DD, DT, and D^3He reaction rates are used to probe the underlying changes in the plasma's temperature and density profiles and are compared with average-ion DUED[4] and kinetic-ion FPION[19] simulations. These measurements during the ICF shock phase are affected by kinetic/multi-ion physics which cannot be accounted for in average-ion-fluid simulations.

This paper is organized as follows: Sec. II describes the experimental setup and diagnostics. Section III compares the measured data with average-ion and kinetic-ion simulations. Section IV discusses interpretation of the data. Section V summarizes the main results and outlines future work.

II. OMEGA EXPERIMENTS

The experiments described in this work are performed on the 60-beam OMEGA laser facility.[25] The targets are spherical and approximately 860 μm in outer diameter, with a thin SiO_2 shell of thickness between 2.2 and 2.7 μm. These targets are filled with different mixtures of D_2, ^{3}He, and T_2 gas and imploded symmetrically using 60 beams with a laser energy of ~14 kJ (at a wavelength of 351 nm) using a 0.6-ns-square pulse shape. The trace amount of tritium in the gas fill provides additional diagnostic measurements (DT yield, ion temperature, and reaction history) without perturbing the implosion. The symmetry of the implosion is improved by phase plates, polarization smoothing, and smoothing by spectral dispersion. In this type of shock-driven implosion (so called because nuclear yields are dominated by shock heating rather than compression), the thin shell is mostly ablated away by the laser, and the implosion begins to disassemble when the rebounding shock reaches the fuel-shell interface. These implosions are ideal for studying ICF shock phase dynamics because they mimic the plasma conditions during the shock phase of more complicated ICF implosions.[5]

In the experiments, DD and DT yields and ion temperatures are measured by neutron time-of-flight[26] diagnostics. The D^{3}He yield and ion temperature are measured using Wedge-Range-Filter proton spectrometers[27] and Charged Particle Spectrometers.[28] The laser absorption (measured using a Full Aperture Back Scatter[29] system) and fuel-shell trajectory (measured using X-ray framing cameras[30]) are used to constrain postshot simulations. The primary observables—DD, DT, and D^{3}He reaction histories—are simultaneously measured using the Particle X-ray Temporal Diagnostic (PXTD)[24] with high relative timing precision (~10 ps). On some shots, the Neutron Temporal Diagnostic[31] provided independent measurements of the DD and/or DT reaction histories.

Data from four shock-driven implosion experiments are discussed in this work, and representative PXTD streak images from the experiments are shown in Fig. 1. The targets and laser drives for all four experiments are approximately the same, but the gas fills are different. These implosions have a burn-averaged Knudsen number of $\langle N_K \rangle$ ~0.3, defined as the burn-averaged ion mean free path (λ_{ii}) over the fuel radius (R_{burn}). PXTD is a scintillator-based, streaked emission history diagnostic, and each of the three scintillator channels is sensitive to X-rays, charged particles, and/or neutrons depending on filtering. The horizontal axis of the streak image is the time axis, and each streak image has either two or three independent scintillator signals (different color lineouts in Fig. 1). Because of the long scintillator decay time (~1.2 ns), the implosion reaction history of interest is encoded in the rising edge of the scintillator signal. The reaction history is extracted using a deconvolution or forward-fitting procedure to remove the instrumental response, transit time broadening in the scintillator, and Doppler broadening. The relative timing uncertainty is ±10 ps between D^{3}He and DT reaction histories. Doppler broadening (a function of diagnostic insertion distance) impacts the DD reaction history more strongly. When the DD reaction history is measured, the relative timing uncertainties are ±20 ps when PXTD is fielded at 9 cm away from the implosion [Fig. 1(a)] and 110 ps when PXTD is fielded at 3 cm away from the implosion [Fig. 1(c)].

The timing difference between the signals on the streak image is related to the times of flight to the detector for different particles. As an example, for a detector at 9 cm away from the target, times of flight

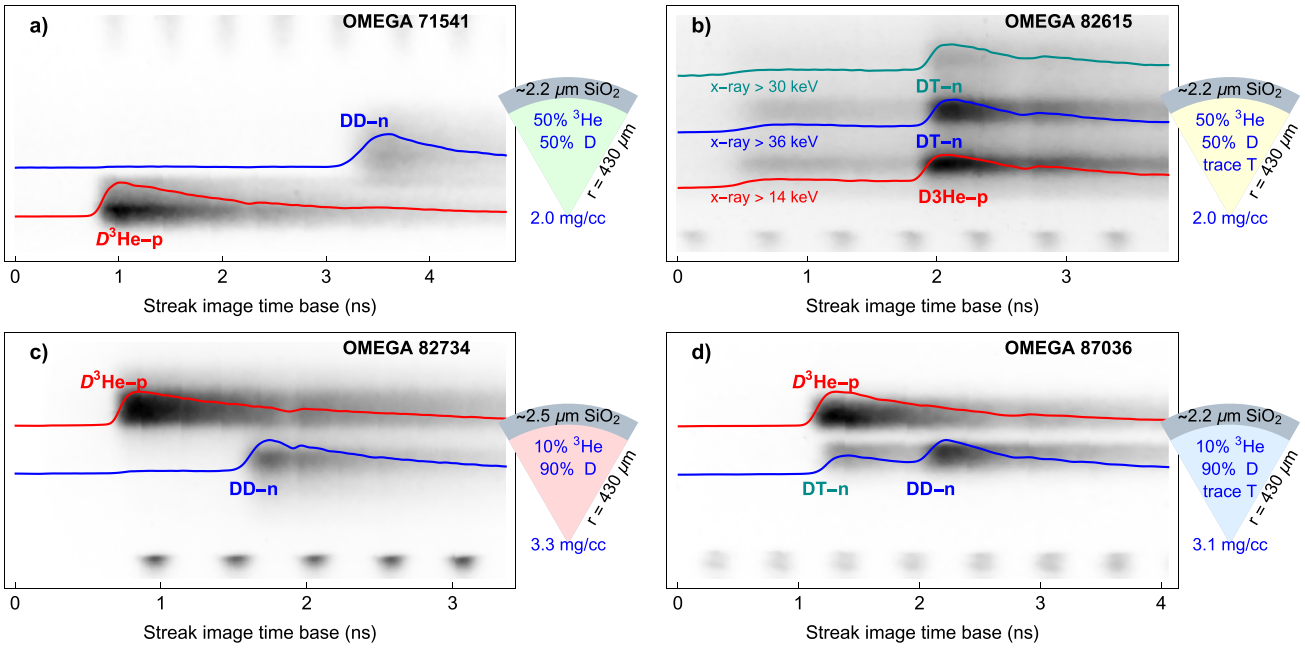

FIG. 1. Representative PXTD streak data, showing (a) DD-n and D^{3}He-p signals in a 50%–50% D^{3}He-gas-filled implosion, (b) DT-n and D^{3}He-p signals in a 50%–50% D^{3}He-gas-filled (with trace T) implosion, (c) DD-n and D^{3}He-p signals in a 90%–10% D^{3}He-gas-filled implosion, and (d) DD-n, DT-n, and D^{3}He-p signals in a 90%–10% D^{3}He-gas-filled (with trace T) implosion. All the gas-fill compositions indicate the atomic percentage. PXTD was fielded at 9 cm away from the target for (a) and (b) and at 3 cm away from the target for (c) and (d).

for DD-n, DT-n, and D^3He-p are ~4.18 ns, 1.78 ns, and 1.74 ns, respectively. These flight times are determined by the birth energies of the particles as well as the measured ion temperatures,[32] and for the D^3He-p, they are assessed through measurements of the D^3He-p energy spectrum. More details of the PXTD diagnostic and analysis are discussed in the instrumentation paper.[24]

The first experiment [Fig. 1(a)] has a 50%–50% D^3He gas fill, and PXTD measured DD and D^3He reaction histories. The second experiment [Fig. 1(b)] has a 50%–50% D^3He gas fill (with trace T), and PXTD measured DT and D^3He reaction histories, as well as X-ray emission histories from the implosion. The X-ray signals and the nuclear signals are separated in time on the streak image because of their different flight times to the detector. The third experiment [Fig. 1(c)] has a 90%–10% D^3He gas fill, and PXTD measured DD and D^3He reaction histories. The fourth experiment [Fig. 1(d)] used an optimized 90%–10% D^3He gas fill (with trace T) that enabled PXTD to measured DD, DT, and D^3He reaction histories. All gas-fill compositions indicate the atomic percentage.

III. DATA AND SIMULATION COMPARISONS

Average-ion hydrodynamic code DUED[4] and Vlasov-Fokker-Planck kinetic-ion code FPION[19] are used to provide further insight into the PXTD data. DUED solves the mass and momentum equations for one averaged ion fluid and separates energy equations for electrons and ions. It includes collisional transport processes (electron-ion coupling, flux-limited electron, and ion conductivities), equations of state, ion viscosity, and multigroup diffusion for radiation. DUED uses the measured laser power for postshot simulations, and adjustment to laser absorption has only a small impact on observables. Two other average-ion hydrodynamic codes LILAC[33] and HYADES[34] have also been used to simulate these implosions with similar results although DUED has the best overall agreement with the measured observables.

FPION implements the Vlasov-Fokker-Planck equations for an arbitrary number of ion species in spherical geometry, treating the lighter fuel ions kinetically and the heavier SiO_2 shell ions (which are expected to be close to local thermal equilibrium) as a fluid. Initializing from average-ion-fluid simulation results, this hybrid kinetic-fluid approach allows treatment of both kinetic ions in the fuel and diffusion across the fuel-shell interface. FPION has been used to simulate similar shock-driven implosions, and more details on the simulation methods are described in Ref. 19.

Figures 2 and 3 summarize the DD, DT, and D^3He nuclear yields, ion temperatures, burnwidths, and differences in nuclear bang times as measured by PXTD and as simulated by DUED and FPION. The bang time is the time of peak nuclear emission. In particular, Fig. 3(a) shows the yield over simulated (YOS) values, calculated as the experimental yield, and divided by either the DUED-simulated or FPION-simulated yield.

Averaging over all four implosion classes and the DD, DT, and D^3He reactions, DUED overpredicts yields by 90%, whereas FPION underpredicts yields by 10%. DUED is able to better match the measured ion temperatures (on average, 1.1 standard deviations away, vs 2.1 standard deviations away for FPION). However, DUED is worse at matching the measured burnwidths (on average, 1.3 standard deviations away, vs 0.9 standard deviations away for FPION). FPION is able to better match the timing differences between reaction histories as compared to DUED although they are still smaller than the measurements.

Four classes of implosions from four different experiments are represented in Figs. 2 and 3. In considering the different experiments, implosions with and without trace T should be considered similar, but not nominally identical, because of systematic differences in targets (shell thickness, etc.) between experiments. For example, a discrepancy is observed for the two implosion types at higher fill density. The increase in the D^3He yield between the implosion types is likely due to the difference in the target thickness, rather than the addition of trace tritium. It is puzzling that FPIONs yield very good agreement for D^3He becomes worse with the addition of trace tritium, as differences in target and laser parameters between implosions are taken into account in the simulations.

Figure 4 shows the DD, DT, and D^3He reaction histories as measured by PXTD and as simulated by DUED and FPION, for the cases of DD/D^3He reaction histories [Fig. 4(a)], DT/D^3He reaction histories [Fig. 4(b)], and DD/DT/D^3He reaction histories [Fig. 4(c)]. In the DUED simulations, the DD, DT, and D^3He reaction histories rise at almost the same time within 10 ps. However, in the PXTD data, the timing difference between the DT and D^3He reaction histories and the timing difference between the DD and D^3He histories are on the order of 40–50 ps, well outside the measurement uncertainty of ±10 ps. Section IV will discuss in more detail the potential mechanisms leading to the differences in these reaction histories. Overall, kinetic-ion FPION simulations are better able to capture the relative timing and reaction rate ratios between DD, DT, and D^3He reactions as compared to the average-ion DUED simulations. FPION-simulated reaction histories also show the same qualitative behaviors as the reaction histories simulated using the Particle-in-Cell code LSP,[10] although FPION is able to better match all the time-integrated and time-resolved measurements.

An important observation is that the DUED-simulated DD and DT reaction histories in these shock-driven implosions [Fig. 4(c)] have almost identical shapes. The similarity between the DD and DT reaction histories is a consequence of the average-ion-fluid assumption in the simulation and the nearly flat DT/DD reactivity ratio near the ion temperature of ~10 keV (Fig. 5). That is, any observed difference between the DD and DT reaction histories in this temperature range [as we see in Fig. 4(c)] is a direct observation of nonaverage-ion-fluid effects.

As there is no significant difference in the measured ion temperatures, burnwidths, and timing differences between implosions with 50%–50% D^3He vs implosions with 90%–10% D^3He and as the observables are repeatable for the same implosion type (Table I in the Appendix), the discussions in the Sec. IV will focus on 90%–10% D^3He (with trace T) implosions for which DD, DT, and D^3He histories are simultaneously measured.

IV. DISCUSSION

Strong shock propagation is inherently a kinetic phenomenon,[20] and can drive differences in ion densities and temperatures (ion species separation and ion temperature decoupling, respectively) in a multi-ion plasma mixture with different masses and charges. FPION simulations for a representative 90%–10% D^3He (with trace T) shock-driven implosion are used in this section. Figure 6 shows the FPION ion density and temperature radial profiles for the D, T, and ^3He ions

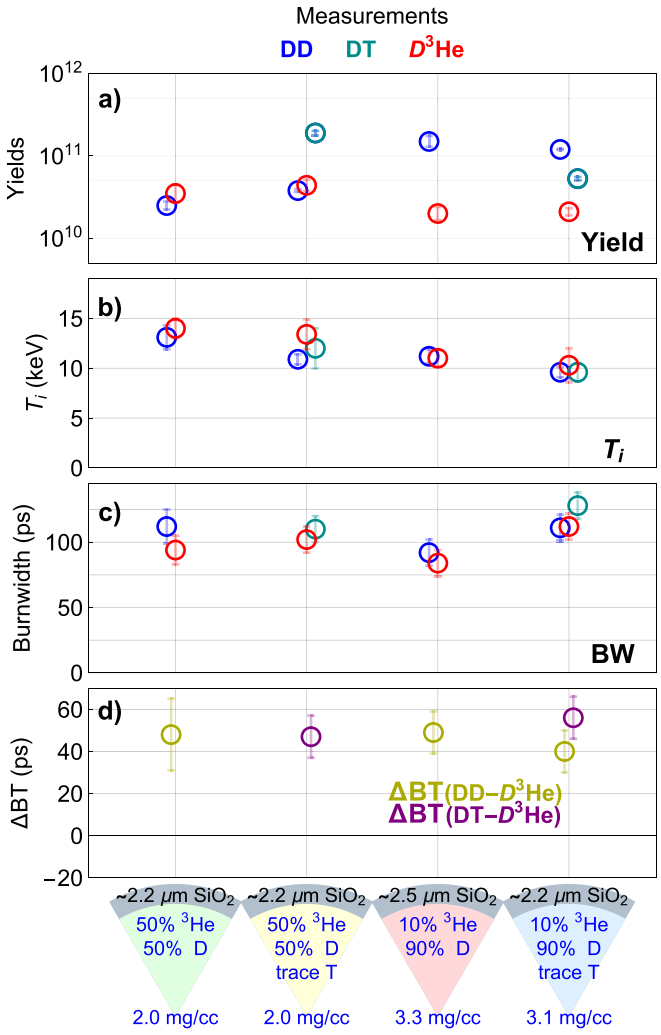

FIG. 2. Measured, averaged (a) nuclear yields, (b) reaction temperatures, (c) burnwidths, and (d) differences in the bang time (time of peak nuclear emission) for four different classes of D^3He-gas-filled (with or without trace T) implosions. Each data point is averaged over 2–4 nominally identical shots. The complete data table is available in the Appendix (Table I).

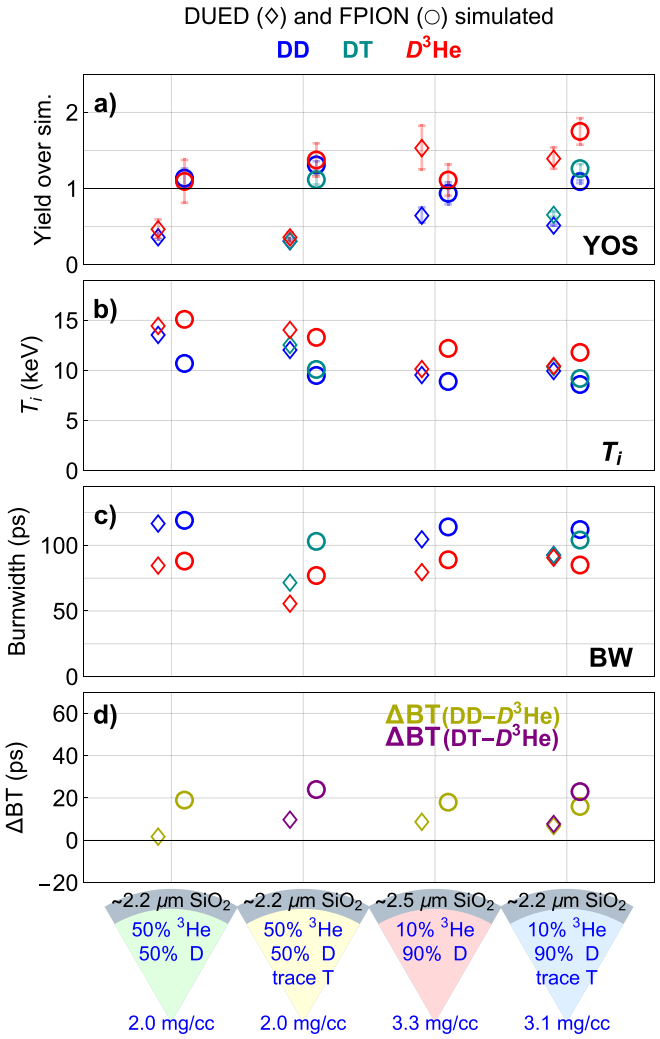

FIG. 3. (a) Measured nuclear yields over simulated (YOS), (b) reaction temperatures, (c) burnwidths, and (d) differences in bang time (time of peak nuclear emission) for four different classes of D^3He-gas-filled (with or without trace T) implosions as simulated by DUED (◇) and FPION (○). The complete data table is available in the Appendix (Table I).

at t = 0.56 ns [Figs. 6(a) and 6(b)] and at t = 0.69 ns [Figs. 6(c) and 6(d)]. As the strong shock propagates inward at t = 0.56 ns, ion density and temperature differences have already developed between the D, T, and ^{3}He ions. The T ions are lagging behind the shock front, and the ^{3}He ions have developed higher temperature than the D ions because of the differences in masses and charges. Later during shock rebound at t = 0.69 ns near the nuclear bang times, these density and temperature differences that evolved during shock convergence have developed into higher ^{3}He ion concentrations and higher ^{3}He and T ion temperatures in the central region of the fuel.

Figure 7 shows density plots of the fractional changes in the (a) ^{3}He/D fuel ratio and (b) ^{3}He/T ratio from the initial fuel ratio, as well as the temperature ratio between (c) ^{3}He and D ions and (d) ^{3}He and T ions. In the density plots, the shock converges at the center at ~0.6 ns, and the nuclear bang times are ~0.7 ns. It is easier to observe in these density plots the higher ^{3}He/D and ^{3}He/T fuel ratio relative to the initial gas-fill ratio near the bang time, as well as the higher ^{3}He and T ion temperatures relative to the D ions.

In turn, these deviations from average-ion density and temperature profiles of the D, T, and ^{3}He ions translate into changes in the DD, DT, and D^3He reaction rates. For a nuclear reaction involving two Maxwellian ion populations at two different temperatures, the effective fusion temperatures[35] for the DD, DT, and D^3He reactions are given by

$$T_{fusion,DD} = T_{i,D}, \tag{1}$$

$$T_{fusion,DT} = \frac{m_T T_{i,D} + m_D T_{i,T}}{m_D + m_T}, \tag{2}$$

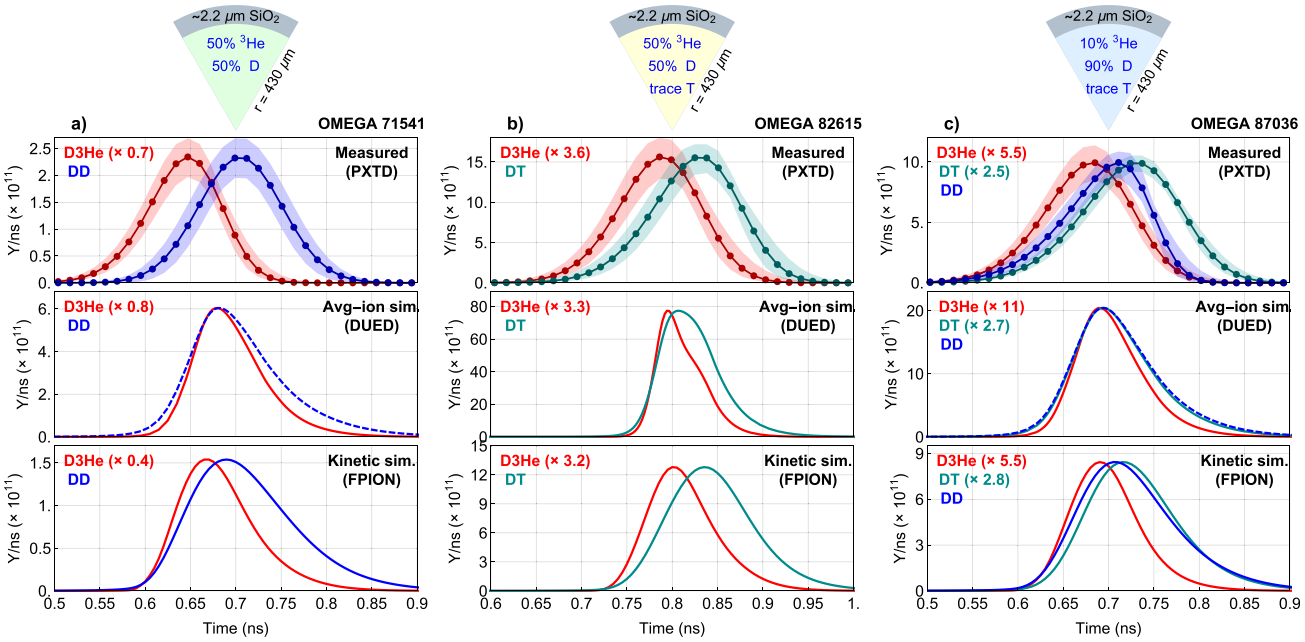

FIG. 4. Comparison between PXTD data, average-ion DUED simulation, and kinetic-ion FPION simulation for (a) DD and D^3He reaction histories in a 50%–50% D^3He-gas-filled implosion, (b) DT and D^3He reaction histories in a 50%–50% D^3He-gas-filled (with trace T) implosion, and (c) DD, DT, and D^3He reaction histories in a 90%–10% D^3He-gas-filled (with trace T) implosion. DD, DT, and D^3He reaction histories are shown in blue, teal, and red, respectively. The absolute time axis is shifted within the measurement uncertainty to better compare with simulations visually. Graphics in (b) are adapted with permission from Sio *et al.* Phys. Rev. Lett. **122**, 035001 (2019). Copyright 2019 American Physical Society.

$$T_{fusion,D^3He} = \frac{m_{^3He}T_{i,D} + m_D T_{i,^3He}}{m_D + m_{^3He}}, \tag{3}$$

where m and T_i are the masses and ion temperatures of the D, T, and ^{3}He ions.

To illustrate how density and temperature differences between ion species can give rise to differences in reaction histories and reaction rate ratios, let us consider several different ways that reaction rates can be calculated. If $n_{i,D}$, $n_{i,T}$, and $n_{i,^3He}$ are fixed to the initial fuel ratio and $T_{i,D} = T_{i,T} = T_{i,^3He}$, the average-ion approximation ($\langle n_i \rangle$, $\langle T_i \rangle$) for the D^3He reaction history is given by

$$Y^{avg\ ion}_{D^3He}(t)/s = \int f_{D,0} f_{^3He,0} \langle n_i \rangle^2 \langle \sigma v \rangle_{D^3He}(\langle T_i \rangle) dV, \tag{4}$$

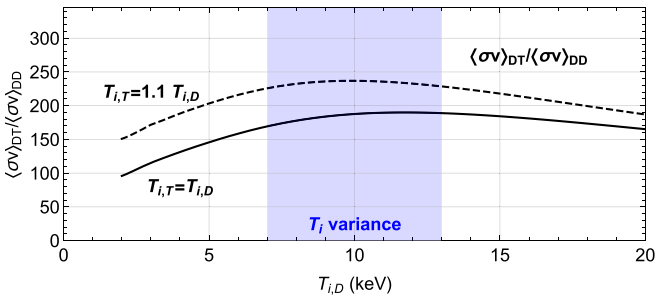

FIG. 5. DT/DD reactivity ratio as a function of deuteron ion temperature if $T_{i,T} = T_{i,D}$ (black) and if $T_{i,T} = 1.1\,T_{i,D}$ (black-dashed). The shaded blue region is the burn-weighted temperature variance (from simulation) for a representative shock-driven implosion discussed in this work.

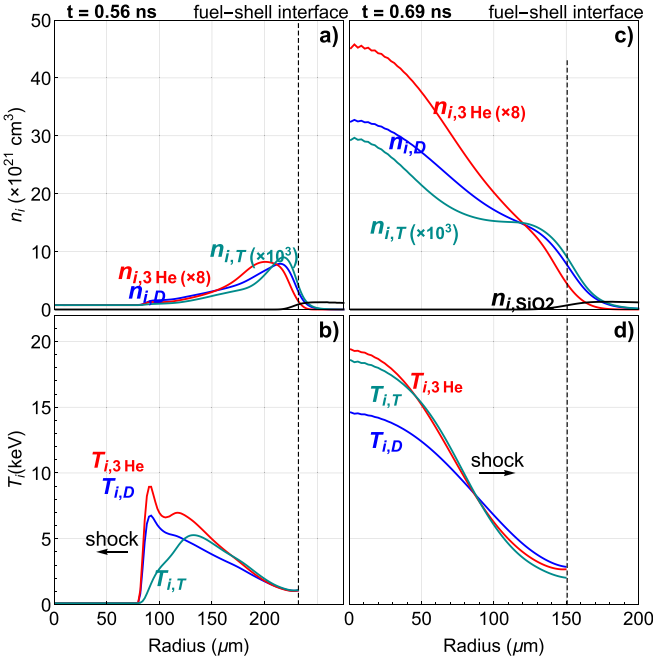

FIG. 6. Kinetic FPION simulation of a 90%–10% D^3He-gas-filled (with trace T) shock-driven implosion, showing density profiles and temperature profiles at t = 0.56 ns during shock convergence (a) and (b) and at t = 0.69 ns during shock rebound (c) and (d). The ^{3}He and T ion densities are scaled to the initial D ion density. Fuel and shell ions can diffuse across the fuel-shell interface (black-dashed line).

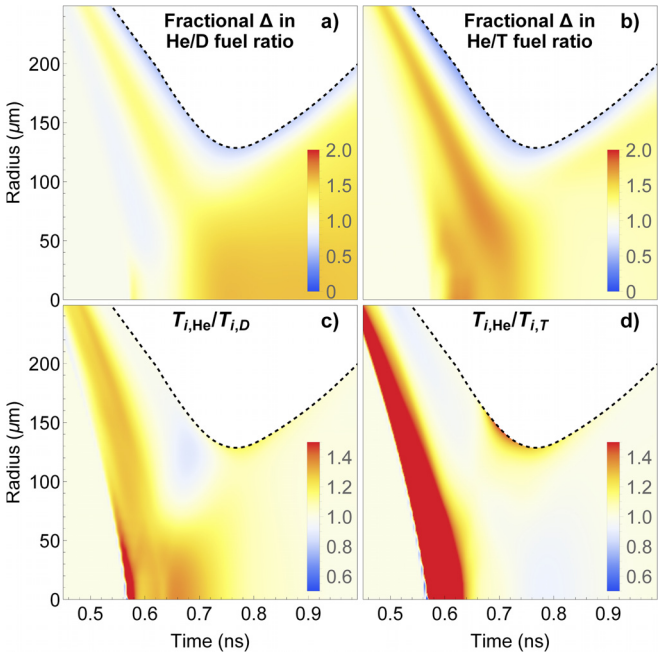

FIG. 7. Kinetic FPION simulation of a 90%–10% D^3He-gas-filled (with trace T) shock-driven implosion, showing (a) fractional change in the $^3He/D$ fuel ratio from the initial fuel ratio, (b) fractional change in the $^3He/T$ fuel ratio from the initial fuel ratio, (c) temperature ratio between ^3He and D ions, and (d) temperature ratio between ^3He and T ions. Fuel and shell ions can diffuse across the fuel-shell interface (black-dashed line).

where $f_{D,0}$ and $f_{^3He,0}$ are the initial fill fraction for D and ^3He, respectively. $\langle n_i \rangle$ and $\langle T_i \rangle$ are the averaged ion density and temperature, and $\langle \sigma v \rangle$ is the Maxwellian-averaged reactivity.

If the density profiles are fixed, but different temperatures between the ions are permitted ($\langle n_i \rangle$, $T_{i,D}$, $T_{i,T}$, $T_{i,^3He}$), the D^3He reaction history is given by

$$Y^{avg\ n_i}_{D^3He}(t)/s = \int f_{D,0} f_{^3He,0} \langle n_i \rangle^2 \langle \sigma v \rangle_{D^3He}(T_{i,D}, T_{i,^3He}) dV. \quad (5)$$

If the density profiles are allowed to vary, but temperatures between the ions are fixed ($n_{i,D}$, $n_{i,T}$, $n_{i,^3He}$, $\langle T_i \rangle$), the D^3He reaction history is given by

$$Y^{avg\ T_i}_{D^3He}(t)/s = \int n_{i,D} n_{i,^3He} \langle \sigma v \rangle_{D^3He}(\langle T_i \rangle) dV. \quad (6)$$

Finally, when each ion species may have different temperature and density profiles ($n_{i,D}$, $n_{i,T}$, $n_{i,^3He}$, $T_{i,D}$, $T_{i,T}$, $T_{i,^3He}$), the D^3He reaction history given by

$$Y^{multi\ ion}_{D^3He}(t)/s = \int n_{i,D} n_{i,^3He} \langle \sigma v \rangle_{D^3He}(T_{i,D}, T_{i,^3He}) dV. \quad (7)$$

Simultaneously measured DD, DT, and D^3He reaction histories provide an unprecedented opportunity to compare time-resolved D^3He/DT, D^3He/DD, and DT/DD reaction rate ratios with average-ion-fluid calculations [Eq. (4)] from DUED simulations, postprocessed multi-ion-fluid calculations [Eq. (7)] from FPION simulations, and kinetic calculations from FPION simulations. These comparisons are summarized in Fig. 8. In the case of the D^3He/DT [Fig. 8(a)] and D^3He/DD [Fig. 8(b)] reaction rate ratios, FPION calculations, kinetic or reduced to multi-ion-fluid, agree much better with the measurements as compared to DUED. The difference between the kinetic and the multi-ion-fluid FPION calculations (purple vs purple-dashed) is also modest, which reflects the hydrodynamiclike ($\langle N_K \rangle \sim 0.3$) plasma conditions in these implosions.

Figure 8(c) shows higher-than-expected measured DT/DD reaction rate ratios at late time, which is not explained by DUED nor FPION. This can also be seen in Fig. 4(c) as a longer measured DT burn relative to DD. One possible explanation for the observation may be higher-than-expected deuteron diffusion out of the burn region relative to tritons, which will decrease the DD reaction rate relative to DT.

However, the multi-ion-fluid calculation [Eq. (7)] does not provide insights into how density and/or temperature deviations from average-ion-fluid models directly impact the reaction rate ratios. Figure 9 provides a way to visualize these impacts by comparing reaction rate ratios assuming an averaged density profile but allowing ion temperature decoupling [Eq. (5), (orange)] and reaction rate ratios assuming an averaged temperature profile but allowing different density profiles [Eq. (6), (green)]. These FPION reaction rate ratios are normalized to the average-ion calculation [Eq. (4), (black horizontal line at 1.0)].

Ion species separation—specifically a higher $^3He/T$ fuel ratio as seen in Figs. 6(c) and 7(b)—has the most direct impact on the D^3He/DT reaction rate ratio [Fig. 9(a)] in FPION simulations. As also seen in Fig. 7(d), near the bang time ($t \sim 0.7$ ns), the temperature difference between ^3He and T ions is small, minimizing the impact on the D^3He/DT reaction rate ratio.

Both ion species separation and ion temperature decoupling contribute to the higher D^3He/DD reaction rate ratio [Fig. 9(b)] in FPION simulations. The higher $^3He/D$ fuel ratio near the bang time [$t \sim 0.7$ ns, Figs. 7(a) and 6(c)] contributes to the higher D^3He/DD reaction rate ratio. At the same time, the higher ^3He ion temperature (relative to D) near the bang time [$t \sim 0.7$ ns, Figs. 7(c) and 6(d)] also contributes to the higher D^3He/DD reaction rate ratio in the FPION simulations.

Finally, differences in both ion densities and temperatures are expected to slightly change the DT/DD reaction rate ratio as compared to the average-ion calculation in the FPION simulations, but these effects are small [Fig. 9(c)].

V. CONCLUSION

In conclusion, multiple reaction histories simultaneously measured using the PXTD in shock-driven implosion experiments with D^3He or D^3He (with trace T) gas fills are used to probe plasma conditions during the shock phase of ICF implosions. These measurements (yields, ion temperatures, bang times, burnwidths, and time-resolved reaction rate ratios) are compared against average-ion DUED and kinetic-ion FPION simulations. On average, FPION is able to better match the measured yields, burnwidths, and timing differences between nuclear bang times (although the FPION-simulated timing differences are still smaller than measured). However, DUED is able to better match the measured ion temperatures. Differences between FPION and data may be a limitation of the hybrid hydro-kinetic approach used by FPION, which relies on initial conditions and trajectories from average-ion-fluid simulations.

This work shows that for relatively hydrodynamiclike implosions ($\langle N_K \rangle \sim 0.3$), average-ion simulations are able to reasonably match

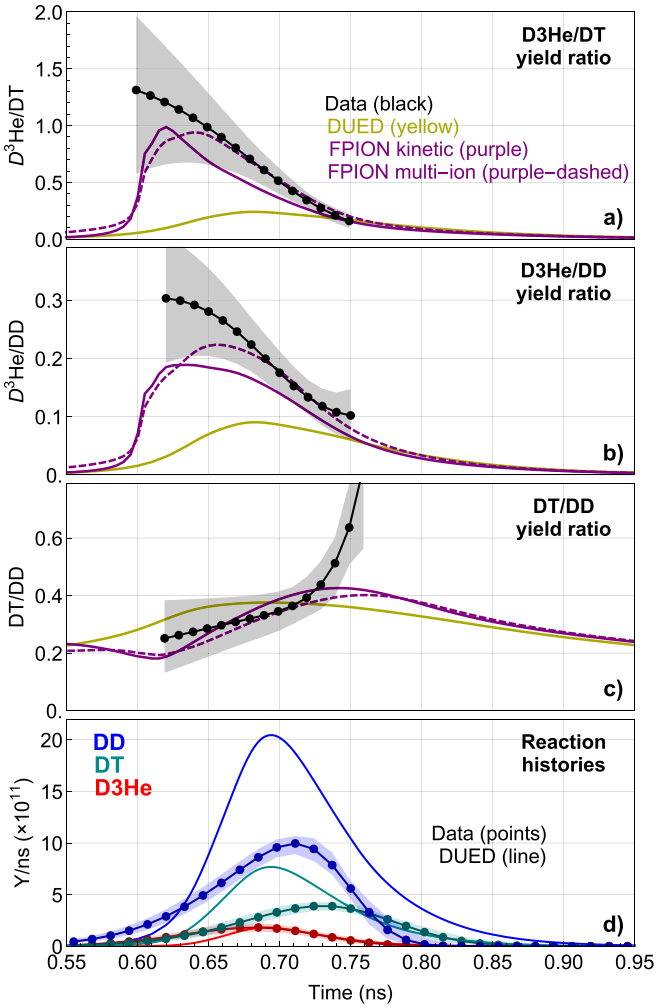

FIG. 8. (a) D^3He/DT reaction rate ratio, (b) D^3He/DD reaction rate ratio, and (c) DT/DD reaction rate ratio as a function of time, as measured by PXTD (black data), as calculated from DUED [yellow, Eq. (4)], as calculated from FPION using kinetic calculations (purple), and as calculated from FPION using multi-ion calculations [purple-dashed, Eq. (7)]. The PXTD-measured reaction rate ratio (black data) is shown with the shaded region denoting the uncertainty. In (d), PXTD-measured (data) and DUED-simulated (line) DD (blue), DT (teal), and D^3He (red) reaction histories are shown as a timing reference.

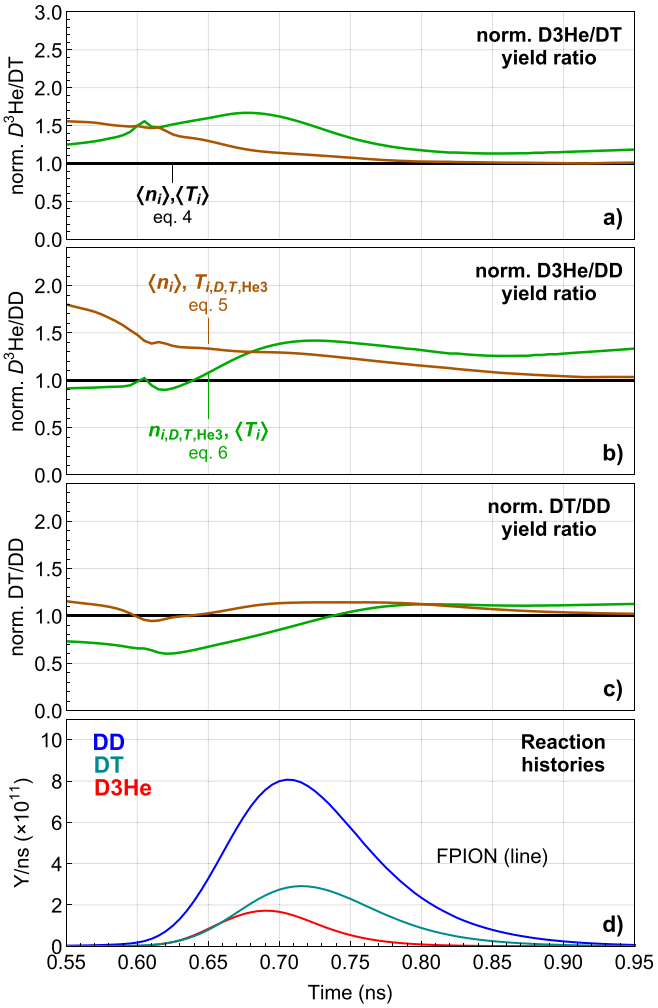

FIG. 9. (a) D^3He/DT reaction rate ratio, (b) D^3He/DD reaction rate ratio, and (c) DT/DD reaction rate ratio as a function of time, normalized to the average-ion expectation. Reaction rate ratios are calculated through different reduction of the FPION profiles: the average-ion expectation [$\langle n_i, T_i \rangle$, black horizontal line at 1.0, Eq. (4)], the average-density expectation [$\langle n_i \rangle$, T_D, T_T, $T_{^3He}$, orange, Eq. (5)], and the average-temperature expectation [$n_{i,D}, n_{i,T}, n_{i,^3He}, \langle T_i \rangle$, green, Eq. (6)]. In (d), FPION-simulated (line) DD (blue), DT (teal), and D^3He (red) reaction histories are shown as a timing reference.

some observables like yields and ion temperatures as well as burnwidths, but not other observables like reaction history timing differences. This is analogous to the conclusion in the study by Rosenberg *et al.*,[36] which found that additional kinetic physics are needed to explain the measured spatially resolved burn profiles in similar shock-driven implosions.

Shock-driven implosions play an important role in understanding how kinetic and multi-ion physics during the shock phase affect implosion performance later during compression when implosion conditions are much more hydrodynamic. For example, during compression, species separation[22] (imprinted from separation during the shock phase), and temperature decoupling[18] have been predicted in kinetic-ion simulations. Very hydrodynamic shock-driven implosions[37] have been tested at the National Ignition Facility (NIF) although NIF lacks a PXTD-type instrument. Future work will focus on probing very kinetic ($N_K \geq 1$) and very hydrodynamic ($N_K \ll 1$) plasma conditions using multiple reaction histories, as well as signatures of kinetic effects (such as thermal decoupling between different ion species) in astrophysical settings.

ACKNOWLEDGMENTS

The authors thank R. Frankel and E. Doeg for contributing to the fielding and processing of CR-39 data used in this work, as well as the OMEGA operations crew for their help in executing these experiments. The targets and gas-fills are coordinated by GA and the LLNL and LLE tritium facilities. This material is based upon the work supported by the Department of Energy, National Nuclear Security

Administration under Award Nos. DE-NA0001857, DE-NA0002949, and DE-NA0002905. This work was also supported in part by NLUF (No. DE-NA0002035). H.S. was supported by a DOE NNSA SSGF fellowship (No. DE-FC52-08NA28752) during this work. S.A. acknowledges Sapienza Project 2016 No. RM11615502006B04, as well as EUROfusion Project Nos. AWP17-ENR-IFE-CEA-01 and ENR-IFE19.CEA-01. This report was prepared as an account of the work sponsored by an agency of the United States Government. Neither the United States Government nor any agency thereof, nor any of their employees, makes any warranty, express or implied, or assumes any legal liability or responsibility for the accuracy, completeness, or usefulness of any information, apparatus, product, or process disclosed, or represents that its use would not infringe privately owned rights. Reference herein to any specific commercial product, process, or service by trade name, trademark, manufacturer, or otherwise does not necessarily constitute or imply its endorsement, recommendation, or favoring by the United States Government or any agency thereof. The views and opinions of the authors expressed herein do not necessarily state or reflect those of the United States Government or any agency thereof.

APPENDIX: DATA AND SIMULATION TABLE

TABLE I. Yields, ion temperatures, bang times, and burnwidths as measured in the experiments and as simulated by DUED and FPION. The uncertainties in the DD, D^3He, and DT yields are UED and FPION. The uncertainties in the DD, Dhe average-ion expect^{3}He, and DT ion temperatures are I0.5 keV, ±2 keV, and ±0.5 keV, respectively. The absolute uncertainty in the bang times (BTs) is ±50 ps. The relative uncertainty between the bang times is ±10 ps (except for shots 70 562, 71 541, and 71 542, with a relative uncertainty of ±20 ps). The uncertainty in the burnwidths (BW) is 15%. OD and ΔR are the outer diameter and shell thickness of the SiO_2 targets, respectively. Information for shot 82 613–82 616 is adapted with permission from Sio *et al.* Phys. Rev. Lett. **122**, 035001 (2019). Copyright 2019 American Physical Society.

	Target						DD				D^3He				DT			
Shot	OD μm	ΔR μm	Frac. D	Frac. ^{3}He	Frac. T	ρ mg/cc	Yield	T_i keV	BT ps	BW ps	Yield	T_i keV	BT ps	BW ps	Yield	T_i keV	BT ps	BW ps
											50%–50% D^3He							
70 562	842	2.2	0.48	0.52	0	2.1	2.3×10^{10}	12.3	754	114	4.0×10^{10}	14.0	704	84				
71 541	866	2.1	0.51	0.49	0	2.0	2.5×10^{10}	13.1	754		3.0×10^{10}	14.0	718	105				
71 542	851	2.1	0.50	0.50	0	2.0	2.7×10^{10}	13.8	705	109	3.6×10^{10}	15.0	648	94				
Experiment average							2.5×10^{10}	13.1	738	112	3.5×10^{10}	14	690	94				
DUED							6.8×10^{10}	13.6	656	117	7.4×10^{10}	14.5	654	85				
FPION							2.2×10^{10}	10.7	694	119	3.2×10^{10}	15.1	675	88				
											50%–50% D^3He, trace T							
82 613	865	2.7	0.51	0.48	0.007	2.0					3.9×10^{10}	13.0	755	108	1.7×10^{11}	14.9	809	121
82 614	889	2.7	0.50	0.49	0.007	2.0	4.0×10^{10}	11.0			5.0×10^{10}	15.4	787	104	2.0×10^{11}	11.6	841	111
82 615	855	2.7	0.50	0.50	0.007	2.0	3.8×10^{10}	10.7			5.0×10^{10}	13.5	789	96	1.9×10^{11}	10.5	831	104
82 616	864	2.7	0.50	0.50	0.007	2.0	3.7×10^{10}	11.1			3.7×10^{10}	11.9	840	101	2.0×10^{11}	10.9	876	102
Experiment average							3.8×10^{10}	10.9			4.4×10^{10}	13.4	793	102	1.9×10^{11}	12.0	839	110
DUED							1.2×10^{11}	12.1			1.2×10^{11}	14.1	810	56	6.0×10^{11}	12.6	820	72
FPION							2.9×10^{10}	9.5			3.2×10^{10}	13.3	834	77	1.7×10^{11}	10.1	858	103
											90%–10% D^3He							
82 731	845	2.5	0.88	0.12	0	3.4	1.3×10^{11}	10.3	750	102	1.5×10^{10}	10.2	691	94				
82 734	889	2.4	0.90	0.10	0	3.3	1.8×10^{11}	11.3	791	89	2.3×10^{10}	10.6	741	79				
82 735	865	2.4	0.88	0.12	0	3.4	1.4×10^{11}	11.8	728	80	2.1×10^{10}	12.0	684	82				
82 745	877	2.6	0.89	0.11	0	3.4	1.7×10^{11}	11.5	734	95	2.2×10^{10}	11.4	693	81				
Experiment average							1.5×10^{11}	11.2	751	92	2.0×10^{10}	11	702	84				
DUED							2.3×10^{11}	9.6	774	105	1.3×10^{10}	10.2	765	80				
FPION							1.6×10^{11}	8.9	789	114	1.8×10^{10}	12.2	771	89				
											90%–10% D^3He, trace T							
87 034	859	2.2	0.89	0.11	0.0009	3.1	1.2×10^{11}	9.6	769	109	2.0×10^{10}	9.1	731	113	5.4×10^{10}	8.9	785	128
87 036	851	2.2	0.89	0.11	0.0009	3.1	1.2×10^{11}	9.6	795	113	2.2×10^{10}	11.5	754	111	5.3×10^{10}	10.2	811	128
Experiment average							1.2×10^{11}	9.6	782	111	2.1×10^{10}	10.3	743	112	5.3×10^{10}	9.6	798	128
DUED							2.3×10^{11}	10.0	745	93	1.5×10^{10}	10.5	738	83	8.0×10^{10}	10.4	745	93
FPION							1.1×10^{11}	8.6	763	112	1.2×10^{10}	11.8	747	85	4.2×10^{10}	9.2	770	104

REFERENCES

[1]S. Park, S. A. Zhekov, D. N. Burrows, G. P. Garmire, and R. McCray, "A Chandra view of the morphological and spectral evolution of supernova remnant 1987A," Astrophys. J. **610**, 275–284 (2004).

[2]J. Lindl, "Development of the indirect-drive approach to inertial confinement fusion and the target physics basis for ignition and gain," Phys. Plasmas **2**, 3933 (1995).

[3]M. M. Marinak, G. D. Kerbel, N. A. Gentile, O. Jones, D. Munro, S. Pollaine, T. R. Dittrich, and S. W. Haan, "Three-dimensional HYDRA simulations of National Ignition Facility targets," Phys. Plasmas **8**, 2275–2280 (2001).

[4]S. Atzeni, A. Schiavi, F. Califano, F. Cattani, F. Cornolti, D. D. Sarto, T. Liseykina, A. Macchi, and F. Pegoraro, "Fluid and kinetic simulation of inertial confinement fusion plasmas," in 2004 Proceedings of the Europhysics Conference on Computational Physics (2005), Vol. 169, pp. 153–159.

[5]M. J. Rosenberg, H. G. Rinderknecht, N. M. Hoffman, P. A. Amendt, S. Atzeni, A. B. Zylstra, C. K. Li, F. H. Séguin, H. Sio, M. G. Johnson, J. A. Frenje, R. D. Petrasso, V. Y. Glebov, C. Stoeckl, W. Seka, F. J. Marshall, J. A. Delettrez, T. C. Sangster, R. Betti, V. N. Goncharov, D. D. Meyerhofer, S. Skupsky, C. Bellei, J. Pino, S. C. Wilks, G. Kagan, K. Molvig, and A. Nikroo, "Exploration of the transition from the hydrodynamiclike to the strongly kinetic regime in shock-driven implosions," Phys. Rev. Lett. **112**, 185001 (2014).

[6]H. W. Herrmann, J. R. Langenbrunner, J. M. Mack, J. H. Cooley, D. C. Wilson, S. C. Evans, T. J. Sedillo, G. A. Kyrala, S. E. Caldwell, C. S. Young, A. Nobile, J. Wermer, S. Paglieri, A. M. Mcevoy, Y. Kim, S. H. Batha, C. J. Horsfield, D. Drew, W. Garbett, M. Rubery, V. Y. Glebov, S. Roberts, and J. A. Frenje, "Anomalous yield reduction in direct-drive deuterium/tritium implosions due to ^{3}He addition," Phys. Plasmas **052706**, 1–9 (2009).

[7]J. R. Rygg, J. A. Frenje, C. K. Li, F. H. Séguin, R. D. Petrasso, J. A. Delettrez, V. Y. Glebov, V. N. Goncharov, D. D. Meyerhofer, S. P. Regan, T. C. Sangster, and C. Stoeckl, "Tests of the hydrodynamic equivalence of direct-drive implosions with different D_2 and ^{3}He mixtures," Phys. Plasmas **13**, 052702 (2006).

[8]H. G. Rinderknecht, M. J. Rosenberg, C. K. Li, N. M. Hoffman, G. Kagan, A. B. Zylstra, H. Sio, J. A. Frenje, M. Gatu Johnson, F. H. Séguin, R. D. Petrasso, P. Amendt, C. Bellei, S. Wilks, J. Delettrez, V. Y. Glebov, C. Stoeckl, T. C. Sangster, D. D. Meyerhofer, and A. Nikroo, "Ion thermal decoupling and species separation in shock-driven implosions," Phys. Rev. Lett. **114**, 025001 (2015).

[9]D. T. Casey, J. A. Frenje, M. Gatu Johnson, M. J.-E. Manuel, H. G. Rinderknecht, N. Sinenian, F. H. Séguin, C. K. Li, R. D. Petrasso, P. B. Radha, J. A. Delettrez, V. Y. Glebov, D. D. Meyerhofer, T. C. Sangster, D. P. McNabb, P. A. Amendt, R. N. Boyd, J. R. Rygg, H. W. Herrmann, Y. H. Kim, and A. D. Bacher, "Evidence for stratification of deuterium-tritium fuel in inertial confinement fusion implosions," Phys. Rev. Lett. **108**, 075002 (2012).

[10]H. Sio, J. A. Frenje, A. Le, S. Atzeni, T. J. T. Kwan, M. Gatu Johnson, G. Kagan, C. Stoeckl, C. K. Li, C. E. Parker, C. J. Forrest, V. Glebov, N. V. Kabadi, A. Bose, H. G. Rinderknecht, P. Amendt, D. T. Casey, R. Mancini, W. T. Taitano, B. Keenan, A. N. Simakov, L. Chacón, S. P. Regan, T. C. Sangster, E. M. Campbell, F. H. Seguin, and R. D. Petrasso, "Observations of multiple nuclear reaction histories and fuel-ion species dynamics in shock-driven inertial confinement fusion implosions," Phys. Rev. Lett. **122**, 035001 (2019).

[11]K. Molvig, N. M. Hoffman, B. J. Albright, E. M. Nelson, and R. B. Webster, "Knudsen layer reduction of fusion reactivity," Phys. Rev. Lett. **109**, 095001 (2012).

[12]P. Amendt, O. L. Landen, H. F. Robey, C. K. Li, and R. D. Petrasso, "Plasma barodiffusion in inertial-confinement-fusion implosions: application to observed yield anomalies in thermonuclear fuel mixtures," Phys. Rev. Lett. **105**, 115005 (2010).

[13]G. Kagan and X.-Z. Tang, "Electro-diffusion in a plasma with two ion species," Phys. Plasmas **19**, 082709 (2012).

[14]N. M. Hoffman, G. B. Zimmerman, K. Molvig, H. G. Rinderknecht, M. J. Rosenberg, A. N. Simakov, H. Sio, A. B. Zylstra, M. G. Johnson, F. H. Séguin, A. Johan, C. K. Li, R. D. Petrasso, D. M. Higdon, G. Srinivasan, V. Y. Glebov, W. Seka, T. C. Sangster, N. M. Hoffman, G. B. Zimmerman, K. Molvig, and H. G. Rinderknecht, "Approximate models for the ion-kinetic regime in inertial-confinement-fusion capsule implosions," Phys. Plasmas **22**, 062702 (2015).

[15]D. R. Welch, D. V. Rose, R. E. Clark, T. C. Genoni, and T. P. Hughes, "Implementation of an non-iterative implicit electromagnetic field solver for dense plasma simulation," Comput. Phys. Commun. **164**, 183–188 (2004).

[16]C. Bellei, P. A. Amendt, S. C. Wilks, M. G. Haines, D. T. Casey, C. K. Li, R. Petrasso, and D. R. Welch, "Species separation in inertial confinement fusion fuels," Phys. Plasmas **20**, 012701 (2013).

[17]A. Le, T. J. T. Kwan, M. J. Schmitt, H. W. Herrmann, and S. H. Batha, "Simulation and assessment of ion kinetic effects in a direct-drive capsule implosion experiment," Phys. Plasmas **23**, 102705 (2016).

[18]A. Inglebert, B. Canaud, and O. Larroche, "Species separation and modification of neutron diagnostics in inertial-confinement fusion," Europhys. Lett. **107**, 65003 (2014).

[19]O. Larroche, H. G. Rinderknecht, and M. J. Rosenberg, "Nuclear yield reduction in inertial confinement fusion exploding-pusher targets explained by fuel-pusher mixing through hybrid kinetic-fluid modeling," Phys. Rev. E **98**, 031201 (2018).

[20]B. D. Keenan, A. N. Simakov, L. Chacón, and W. T. Taitano, "Deciphering the kinetic structure of multi-ion plasma shocks," Phys. Rev. E **96**, 053203 (2017).

[21]B. D. Keenan, A. N. Simakov, W. T. Taitano, and L. Chacn, "Ion species stratification within strong shocks in two-ion plasmas," Phys. Plasmas **25**, 032103 (2018).

[22]W. T. Taitano, A. N. Simakov, L. Chacn, and B. Keenan, "Yield degradation in inertial-confinement-fusion implosions due to shock-driven kinetic fuel-species stratification and viscous heating," Phys. Plasmas **25**, 056310 (2018).

[23]S. C. Hsu, T. R. Joshi, P. Hakel, E. L. Vold, M. J. Schmitt, N. M. Hoffman, R. M. Rauenzahn, G. Kagan, X.-Z. Tang, R. C. Mancini, Y. Kim, and H. W. Herrmann, "Observation of interspecies ion separation in inertial-confinement-fusion implosions," Europhys. Lett. **115**, 65001 (2016).

[24]H. Sio, J. A. Frenje, J. Katz, C. Stoeckl, D. Weiner, M. Bedzyk, V. Glebov, C. Sorce, M. G. Johnson, H. G. Rinderknecht, A. B. Zylstra, T. C. Sangster, S. P. Regan, T. Kwan, A. Le, A. N. Simakov, W. T. Taitano, L. Chacón, B. Keenan, R. Shah, G. Sutcliffe, and R. D. Petrasso, "A particle x-ray temporal diagnostic (PXTD) for studies of kinetic, multi-ion effects, and ion-electron equilibration rates in inertial confinement fusion plasmas at OMEGA (invited)," Rev. Sci. Instrum. **87**, 11D701 (2016).

[25]T. Boehly, D. Brown, R. Craxton, R. Keck, J. Knauer, J. Kelly, T. Kessler, S. Kumpan, S. Loucks, S. Letzring, F. Marshall, R. McCrory, S. Morse, W. Seka, J. Soures, and C. Verdon, "Initial performance results of the OMEGA laser system," Opt. Commun. **133**, 495–506 (1997).

[26]V. Y. Glebov, C. J. Forrest, K. L. Marshall, M. Romanofsky, T. C. Sangster, M. J. Shoup, and C. Stoeckl, "A new neutron time-of-flight detector for fuel-areal-density measurements on omega," Rev. Sci. Instrum. **85**, 11E102 (2014).

[27]F. H. Séguin, N. Sinenian, M. Rosenberg, A. Zylstra, M. J.-E. Manuel, H. Sio, C. Waugh, H. G. Rinderknecht, M. G. Johnson, J. Frenje, C. K. Li, R. Petrasso, T. C. Sangster, and S. Roberts, "Advances in compact proton spectrometers for inertial-confinement fusion and plasma nuclear science," Rev. Sci. Instrum. **83**, 10D908 (2012).

[28]F. H. Séguin, J. A. Frenje, C. K. Li, D. G. Hicks, S. Kurebayashi, J. R. Rygg, B. E. Schwartz, R. D. Petrasso, S. Roberts, J. M. Soures, D. D. Meyerhofer, T. C. Sangster, J. P. Knauer, C. Sorce, V. Y. Glebov, C. Stoeckl, T. W. Phillips, R. J. Leeper, K. Fletcher, and S. Padalino, "Spectrometry of charged particles from inertial-confinement-fusion plasmas," Rev. Sci. Instrum. **74**, 975 (2003).

[29]W. Seka, D. H. Edgell, J. P. Knauer, J. F. Myatt, A. V. Maximov, R. W. Short, T. C. Sangster, C. Stoeckl, R. E. Bahr, R. S. Craxton, J. A. Delettrez, V. N. Goncharov, I. V. Igumenshchev, and D. Shvarts, "Time-resolved absorption in cryogenic and room-temperature direct-drive implosions," Phys. Plasmas **15**, 056312 (2008).

[30]F. J. Marshall, P. W. McKenty, J. A. Delettrez, R. Epstein, J. P. Knauer, V. A. Smalyuk, J. A. Frenje, C. K. Li, R. D. Petrasso, F. H. Séguin, and R. C. Mancini, "Plasma-density determination from x-ray radiography of laser-driven spherical implosions," Phys. Rev. Lett. **102**, 185004 (2009).

[31]C. Stoeckl, R. Boni, F. Ehrne, C. J. Forrest, V. Y. Glebov, J. Katz, D. J. Lonobile, J. Magoon, S. P. Regan, M. J. Shoup, A. Sorce, C. Sorce, T. C. Sangster, and D. Weiner, "Neutron temporal diagnostic for high-yield deuterium-tritium cryogenic implosions on OMEGA," Rev. Sci. Instrum. **87**, 053501 (2016).

[32]L. Ballabio, J. Kllne, and G. Gorini, "Relativistic calculation of fusion product spectra for thermonuclear plasmas," Nucl. Fusion **38**, 1723–1735 (1998).

[33]J. Delettrez, "Thermal electron transport in direct-drive laser fusion," Can. J. Phys. **64**, 932–943 (1986).
[34]J. T. Larsen and S. M. Lane, "HYADES: A plasma hydrodynamics code for dense plasma studies," J. Quant. Spectrosc. Radiat. Transfer **51**, 179–186 (1994).
[35]H. Brysk, "Fusion neutron energies and spectra," Plasma Phys. **15**, 611 (1973).
[36]M. J. Rosenberg, F. H. Sguin, P. A. Amendt, S. Atzeni, H. G. Rinderknecht, N. M. Hoffman, A. B. Zylstra, C. K. Li, H. Sio, M. Gatu Johnson, J. A. Frenje, R. D. Petrasso, V. Y. Glebov, C. Stoeckl, W. Seka, F. J. Marshall, J. A. Delettrez, T. C. Sangster, R. Betti, S. C. Wilks, J. Pino, G. Kagan, K. Molvig, and A. Nikroo, "Assessment of ion kinetic effects in shock-driven inertial confinement fusion implosions using fusion burn imaging," Phys. Plasmas **22**, 062702 (2015).
[37]S. Le Pape, L. Divol, L. B. Hopkins, A. Mackinnon, N. B. Meezan, D. Casey, J. Frenje, H. Herrmann, J. McNaney, T. Ma, K. Widmann, A. Pak, G. Grimm, J. Knauer, R. Petrasso, A. Zylstra, H. Rinderknecht, M. Rosenberg, M. Gatu-Johnson, and J. D. Kilkenny, "Observation of a reflected shock in an indirectly driven spherical implosion at the National Ignition Facility," Phys. Rev. Lett. **112**, 225002 (2014).